P4.3 A LAGRANGIAN TURBULENT TRANSPORT MODEL OF EVOLVING SEA-SPRAY DROPLETS OVER THE OCEAN

James A. Mueller* and Fabrice Veron

University of Delaware, College of Marine Studies

1. INTRODUCTION

Sea-spray contributes to the momentum, mass, heat, and moisture transfer between the ocean and the atmosphere. Although the direction of these fluxes is generally known, their magnitudes remain unclear. Sea-spray is predominantly formed through two mechanisms. The first mechanism, resulting in film or jet droplets, is the ejection of water droplets into the air from bursting bubbles at the surface. The magnitude of their radii is on the order of O(1-10) mm. The second mechanism, resulting in spume droplets, is the forceful separation of water particles at the top of waves caused by sufficiently strong winds. The magnitude of spume droplet radii is on the order of O(10-1000) mm. Because of their relative size, spume droplets have the potential to transfer considerably more mass, momentum, heat, and moisture than jet or film droplets. While the potential is greater, intuition suggests that the resident time of spume droplets will be shorter due to their faster settling velocities and vastly different ejection mechanism. Therefore, it seems necessary to gain a greater understanding of both the microphysics and the transport of sea-spray droplets, spume droplets in particular. Numerous studies (e.g. Rouault et al., 1991; Andreas, 1992; Edson and Fairall, 1994; Andreas, 1995; Andreas et al., 1995; Edson et al., 1996; Mestayer et al., 1996; Makin, 1998; Andreas and Emanuel, 2001; Van Eijk et al., 2001; Meirink, 2002) have appropriately investigated the microphysics and transport of sea-spray droplets. There has, however, been a lack of exclusively Lagrangian models, which simultaneously solve the microphysical evolution of the droplets during their transport through the marine boundary layer. Our Spray Lagrangian Turbulent Transport and Evolution (SpLaTTE) model is an attempt to fill the aforementioned void.

2. MODEL

The SpLaTTE model is a Monte-Carlos type simulation, which follows individual droplets from ejection into the air until they reenter the ocean or attain a quasi-equilibrium state. The model includes a realistic surface wave spectrum, forming the bottom boundary. While suspended in the air, the droplet traverses an atmospheric boundary layer that includes a viscous sublayer, a wave boundary layer (WBL), and a stratified log layer. In addition, the droplet is subjected to turbulent velocities and turbulent scalars following the Kolmogorov-Obukhov-Corrsin theory. Furthermore, the droplet's velocity and evolution are solved using the complete, linear, unsteady equation of motion (Hinze, 1975) and the complete microphysical equations (Pruppacher and Klett, 1978; Andreas, 2005), respectively. While the model is computationally expensive, it provides new insight into the properties of the droplets that reenter the oceanic surface via the viscous sublayer and WBL.

* *Corresponding author address:* James A. Mueller, University of Delaware, Air-sea Interaction Laboratory, 002 Robinson Hall, Newark, DE 19716; JMueller@udel.edu

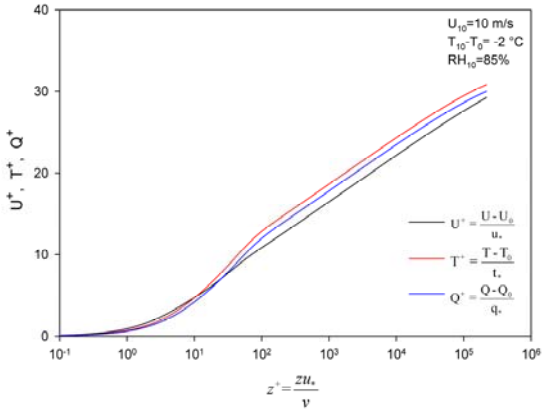

Figure 1. Profiles for velocity (black), temperature (red), and water vapor (blue) in wall coordinates

2.1 *Profiles*

What happens to the droplets as they reenter the ocean is strongly dependent on the mean atmospheric conditions near the surface. Therefore, the viscous, thermal, and water vapor sublayers cannot be neglected. Figure 1 shows sample profiles in wall coordinates that include the linear sublayers in addition to the standard log layers for velocity, temperature, and water vapor. In this case the 10-meter wind speed of 10 m/s and the corresponding surface wave spectrum fall in the transitionally rough regime. Therefore, the viscous sublayer is expected to smaller than for the case of smooth flow over a flat wall. The thermal and water vapor sublayers appear larger than expected because viscosity is used for the non-dimensionalization of height rather than thermal and water vapor diffusivities, respectively. Furthermore, since there is no analog of smooth and rough regimes for passive scalars, the profiles for temperature and water vapor in wall coordinates only change slightly as wind and surface

conditions vary. The same is certainly not true for the velocity profiles. For a recent review of rough flow, see Jiménez (2004).

Figure 2 shows the neutral transfer coefficients for velocity, temperature, and water vapor as a function of wind speed at 10 meters. The roughness length for the velocity profile was parameterized by manipulating the Charnock coefficient so that the drag coefficient matched data at high wind speeds (Powell et al., 2003; Donelan et al., 2004). The temperature and water vapor roughness lengths are modified forms of those found in Garratt (1992) and Meirink and Makin (2001) so that the constant flux assumption holds. Also, note that the drag coefficient is less than expected at lower wind speeds due to the presence of the viscous sublayer.

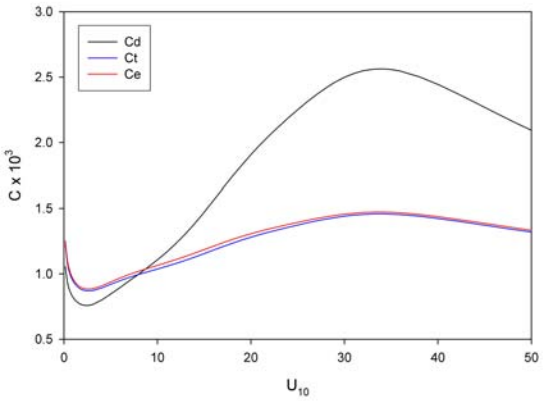

Figure 2. Transfer Coefficients for momentum, temperature, and water vapor as a function of 10-m wind speed

2.2 *Wave Boundary Layer (WBL)*

The presence of waves causes the flow to deviate from smooth flow and actually become transitionally rough for most wind speeds. Consequently, the size of the viscous sublayer decreases as the flow becomes rougher, which generally occurs as the wind speed increases. In order to maintain a constant stress assumption, the turbulent stresses are necessarily damped in the WBL as well. The total stress at a particular wind speed, however, is almost always greater than the smooth flow equivalent because of the form drag due to the wavy surface and therefore, can be divided into three components:

$$\tau = \tau_v + \tau_w + \tau_t, \qquad (1)$$

where the subscripts *v*, *w*, and *t* represent the molecular viscosity, wave-induced, and turbulent components of the total stress, respectively.

The viscous component of the stress is known at every height and is

$$\tau_v = \mu \frac{\partial U}{\partial z}, \qquad (2)$$

where μ is molecular viscosity and $\partial U/\partial z$ is the vertical gradient of the mean velocity. The wave-induced stress at the top of the viscous sublayer is found by taking the difference between the total stress and the stress of the smooth flow limit. The smooth flow limit is expected to be an upper bound for tangential stress (Banner and Peirson, 1998). The wave-induced stress decays as

$$\tau_w(z) = \tau_w(z^+)\left(1 - \frac{\tau_v}{\tau}\right) F(z - z^+), \qquad (3)$$

where z^+ is the height of the viscous sublayer and

$$F(z - z^+) = e^{-\frac{z - z^+}{li}} \cos\left(\frac{\pi(z - z^+)}{2li}\right), \qquad (4)$$

when $z - z^+ \geq 0$ and $F(z - z^+) = 1$ when $z - z^+ < 0$ (Makin and Kudryavtsev, 1999). The decay length scale, *li*, is the height of the inner region (Belcher and Hunt, 1998). Figure 3 shows the ratio of each stress component to the total stress when the 10-m wind speed is 10 m/s. For this wind speed and corresponding wave age, the fraction of the wave-induced stress to the total stress at the top of the viscous sublayer is approximately 0.45.

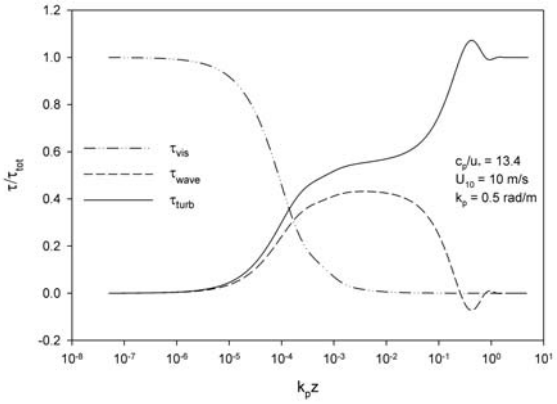

Figure 3. Fraction of each stress component to the total stress as a function of k_pz, where k_p is the significant wavenumber. The components are the viscous (dash-dotted), wave-induced (dashed), and Reynolds (solid) stresses.

2.3 *Turbulence*

In addition to the changing mean atmospheric conditions surrounding the droplet as it is transported, there are also turbulent components of the flow. Therefore, the droplet can never truly be in static equilibrium. Presently, the model incorporates fluctuating horizontal and vertical velocities as well as fluctuating temperatures and water vapor concentrations. The turbulent velocity quantities are

treated as anisotropic, i.e. the horizontal and vertical characteristics are different (see figure 4). Furthermore, the turbulent temperature and water vapor concentration quantities are modeled as passive scalars. All of the fluctuating quantities are additionally coupled with the vertical fluctuations. For a recent review of passive scalar turbulence, see Warhaft (2000), and for Lagrangian turbulence, see Yeung (2002).

Figure 4 shows sample time series of the fluctuating horizontal and vertical velocities in addition to the instantaneous product, *u'w'*. The normalized means and standard deviations for the run are also included, where u_* is the friction velocity and σ denotes the standard deviation.

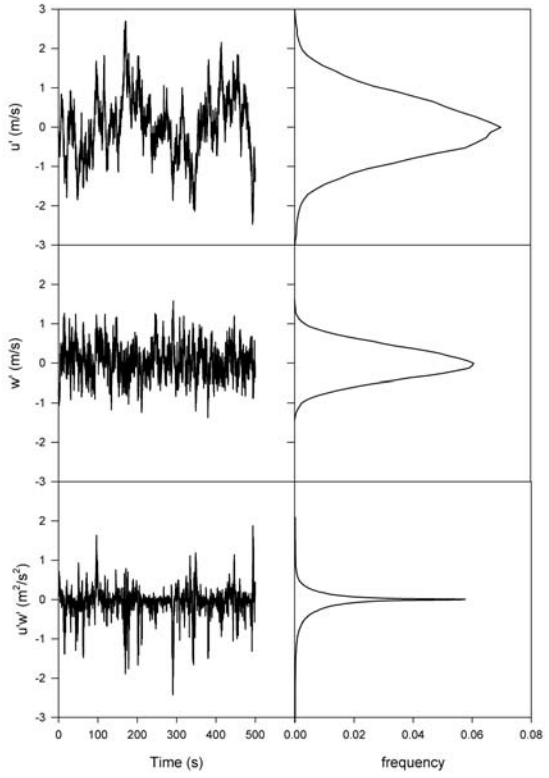

$\frac{\overline{u'}}{u_*}$	$\frac{\overline{w'}}{u_*}$	$\frac{\overline{u'w'}}{u_*^2}$	$\frac{\sigma_u}{u_*}$	$\frac{\sigma_w}{u_*}$	$\frac{\sigma_{uw}}{u_*^2}$
0.0259	0.0291	-0.753	2.378	1.253	3.126

Figure 4. Sample time series (500 s out of 4620 s) of the turbulent velocities and instantaneous product as well as the frequency of each value, i.e. the number of occurrences divided by *n* = 462000 iterations

3. RESULTS

Our preliminary results suggest that typical simplifications in previous models lead to an overestimation of the heat and moisture fluxes due to sea-spray. In fact, the temperature of sea-spray droplets seems to move rapidly toward the surface temperature as they fall back into the ocean. Most models assume that the sensible heat flux of the droplet occurs instantaneously. Additionally, they approximate the latent heat flux based on results from full microphysical runs under simplified, constant conditions. Figure 5 shows the static temperature of 100 μm droplets at surface and 10-meter conditions and sample evolutions during transport. Notice that the droplets move toward the surface conditions quickly as they reenter through the near surface layer. Thus, it appears that solving the full microphysical equations simultaneously with the transport model does provide new insight regarding the properties of the sea-spray droplets that reenter the ocean.

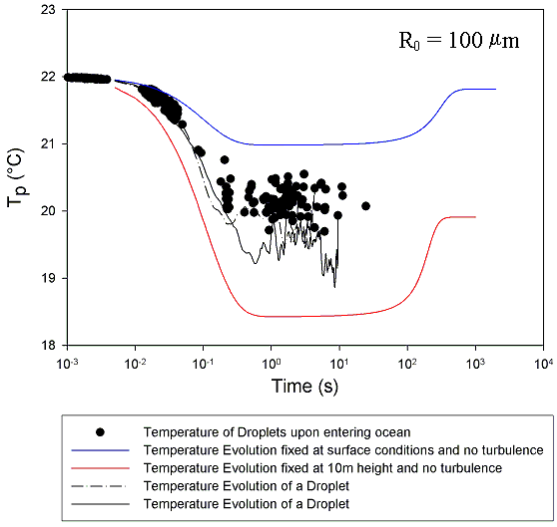

Figure 5. The temperature evolution of droplets with an initial radius of 100 μm under static conditions (red and blue lines) as well as sample runs within the turbulent transport model (solid black line and dash-dotted line)

4. FUTURE WORK

Although the model is computationally expensive, preliminary results motivate further investigation. Individual components of the model have been verified with previous studies, and the model seems to be quite robust. Thus, the natural next step is to see exactly how spray droplets affect the transfer of momentum, heat, and moisture between the air and the sea. Admittedly, the lack of feedback effects is a major limitation, but there are plans to develop a parameterization for those effects as well.

5. REFERENCES

Andreas, E., 1992: Sea spray and the turbulent air-sea heat fluxes. *J. Geophys. Res.*, **97**, 11429-11441.

Andreas, E., 1995: The temperature of evaporating sea spray droplets. *J. Atmos. Sci.*, **52**, 852-862.

Andreas, E., 2005: Approximation formulas for the microphysical properties of saline droplets. *Atmos. Res.*, **75**, 323-345.

Andreas, E., J. Edson, E. Monahan, M. Rouault, and S. Smith, 1995: The spray contribution to net evaporation from the sea – A review of recent progress. *Bound.-Layer Meteor.*, **72**, 3-52.

Andreas, E. and K. Emanuel, 2001: Effects of sea spray on tropical cyclone intensity. *J. Atmos. Sci.*, **58**, 3741-3751.

Banner, M. and W. Peirson, 1998: Tangential stress beneath wind-driven air-water interfaces. *J. Fluid Mech.*, **364**, 115-145.

Belcher, S. and J. Hunt, 1998: Turbulent flow over hills and waves. *Annu. Rev. Fluid Mech.*, **30**, 507-538.

Donelan, M. A., B. K. Haus, N. Reul, W. J. Plant, M. Stiassnie, H. C. Graber, O. B. Brown, and E. S. Saltzman, 2004: On the limiting aerodynamic roughness of the ocean in very strong winds. *Geophys. Res. Lett.*, **31**, L18306.

Edson, J. and C. Fairall, 1994: Spray droplet modeling.1. Lagrangian model simulation of the turbulent transport of evaporating droplets. *J. Geophys. Res.*, **99**, 25295-25311.

Edson, J., S. Anquetin, P. Mestayer, and J. Sini, 1996: Spray droplet modeling.2. An interactive Eulerian-Lagrangian model of evaporating spray droplets. *J. Geophys. Res.*, **101**, 1279-1293.

Garratt, J. R., 1992: The atmospheric boundary layer. Cambridge atmospheric and space science series, Cambridge University Press, xviii, 316 pp.

Hinze, J. O., 1975: *Turbulence*. 2d ed. McGraw-Hill, x, 790 pp.

Jiménez, J., 2004: Turbulent flows over rough walls. *Annu. Rev. Fluid Mech.*, **36**, 173-96.

Makin, V., 1998: Air-sea exchange of heat in the presence of wind waves and spray. *J. Geophys. Res.*, **103**, 1137-1152.

Makin, V. K. and V. N. Kudryavtsev, 1999: Coupled sea surface-atmosphere model - 1. Wind over waves coupling. *J. Geophys. Res.*, **104**, 7613-7623.

Meirink, J., 2002: The Role of Wind Waves and Sea Spray in Air-Sea Interaction. Ph.D. Thesis, Technische Universiteit Delft, 161.

Meirink, J. and V. Makin, 2001: The impact of sea spray evaporation in a numerical weather prediction model. *J. Atmos. Sci.*, **58**, 3626-3638.

Mestayer, P., A. VanEijk, G. DeLeeuw, and B. Tranchant, 1996: Numerical simulation of the dynamics of sea spray over the waves. *J. Geophys. Res.*, **101**, 20771-20797.

Powell, M. D., P. J. Vickery, and T. A. Reinhold, 2003: Reduced drag coefficient for high wind speeds in tropical cyclones. *Nature*, **422**, 279-283.

Pruppacher, H. R. and J. D. Klett, 1978: *Microphysics of clouds and precipitation*. D. Reidel Pub. Co., xiv, 714 pp.

Rouault, M., P. Mestayer, and R. Schiestel, 1991: A model of evaporating spray droplet dispersion. *J. Geophys. Res.,* **96**, 7181-7200.

Van Eijk, A., B. Tranchant, and P. Mestayer, 2001: SeaCluse: Numerical simulation of evaporating sea spray droplets. *J. Geophys. Res.*, **106**, 2573-2588.

Warhaft, Z., 2000: Passive scalars in turbulent flows. *Annu. Rev. Fluid Mech.*, **32**, 203-240.

Yeung, P., 2002: Lagrangian investigations of turbulence. *Annu. Rev. Fluid Mech.*, **34**, 115-142